We are IntechOpen,
the world's leading publisher of
Open Access books
Built by scientists, for scientists

6,900
Open access books available

186,000
International authors and editors

200M
Downloads

Our authors are among the

154
Countries delivered to

TOP 1%
most cited scientists

12.2%
Contributors from top 500 universities

CLARIVATE ANALYTICS

BOOK CITATION INDEX

INDEXED

WEB OF SCIENCE™

Selection of our books indexed in the Book Citation Index
in Web of Science™ Core Collection (BKCI)

Interested in publishing with us?
Contact book.department@intechopen.com

Numbers displayed above are based on latest data collected.
For more information visit www.intechopen.com

9

Two Novel Induction Heating Technologies: Transverse Flux Induction Heating and Travelling Wave Induction Heating

Youhua Wang[1], Junhua Wang[2], S. L. Ho[2], Xiaoguang Yang [1], and W. N. Fu[2]
*[1]Province-Ministry Joint Key Laboratory of Electromagnetic Field and Electrical
Apparatus Reliability, Hebei University of Technology, Tianjin
[2]Department of Electrical Engineering, The Hong Kong
Polytechnic University, Kowloon
[1]China
[2]Hong Kong*

1. Introduction

The increasing demand for industrial furnace heaters has attracted a lot of attentions from researchers and practitioners. Traditional longitudinal method is inadequate to meet the ever increasing demand on quality performance in regard to temperature uniformity on the work strips, especially on thin and long strips. Among the new systems being developed recently, transverse flux induction heating (TFIH) and the traveling wave induction heating (TWIH) processes are potentially very promising and attractive.

Longitudinal induction heating was the most often used method in the past and it is still used today. However, there are many disadvantages of the traditional induction heating method. It is well known that we can increase the operational frequency to decrease the skin depth in order to increase the heating efficiency. For the metal strip with certain depth, 10 kHz or above frequency has to be used if using longitudinal induction heating method. The traditional induction heating method can only applied to metal strips with large thickness.

TFIH is prior to the conventional axial flux induction heating in many aspects, e.g. lower frequency for thin strips. But the temperature distribution is more complex such as may higher at one place but lower at the other across the entire strip width. The fundamental principles of the TWIH are known for many years [1-3]. TWIH, as one of the multiphase induction heating systems, has particular features which make them attractive for application to some heating and melting processes in industry. Among the advantages we can mention the possibility to heat quite uniformly thin strips or regions of a body without moving the inductor above its surface, to reduce the vibrations of inductor and load due to the electro-dynamic forces and also the noise provoked by them, to obtain nearly balanced distributions of power and temperature [4].

In this chapter these two different novel types – TFIH and TWIH technologies are considered. Some standard and specially developed FEM codes based on numerical methods were successfully used for the study of TFIH and TWIH heaters. The main advantages and the particular characteristics of TFIH and TWIH systems such as the effect

of slots on induced power distributions were studied. The FEM codes and the results of numerical simulation may be therefore used easily and reliably, for the design of these two systems. While TFIH systems have been studied for many years, TWIH systems are not yet fully appreciated with respect to their main advantages and possible industrial applications [1, 2].

2. Transverse Flux Induction Heating (TFIH)

Transverse flux induction heating (TFIH) is prior to the conventional axial flux induction heating in many aspects, e.g. lower frequency for thin strips. But the temperature distribution is more complex such as may higher at one place but lower at the other across the entire strip width. It is influenced by the inductor structure, which must be optimized. Considering the long computation time, Optimization is done through orthogonal experiment. The design of the TFIH equipment necessitates accurate prediction for the thermal characteristic. So it is essential to obtain a clear understanding of the eddy current in the workpiece and further more the power losses in temperature field [5, 6].

The mathematical model for this sinusoidal quasi-static eddy current problem results from the Maxwell equations and is described by the complex magnetic vector potential $\underline{A}$ and an electrical complex scalar potential $\underline{\phi}$.

$$rot\,\frac{1}{\mu}\,rot\,\vec{\underline{A}} - grad(\frac{1}{\mu}rot\underline{A}) + j\,\omega\kappa\left(\vec{\underline{A}} + grad\,\underline{\phi}\right) = \kappa\vec{\underline{E}}_S \tag{1}$$

where $\vec{\underline{E}}_s$ is the electric field strength impressed by the power source. The requirement of a zero divergence condition of current density must be fulfilled:

$$\mathrm{div}\left(\kappa\vec{\underline{A}} + \kappa\mathrm{grad}\underline{\phi}\right) = 0 \tag{2}$$

The eddy current density is computed with

$$\vec{\underline{J}} = j\,\omega\kappa\left(\vec{\underline{A}} + grad\,\underline{\phi}\right) + \kappa\vec{\underline{E}}_S \tag{3}$$

And it determines the heat source distribution:

$$p_v = \left|\vec{\underline{J}}^2\right| / k \tag{4}$$

The temperature field $\vartheta(x,y,z)$ is computed based on the Fourier's thermal conduction equation,

$$\frac{\partial(c\,\rho\,\vartheta)}{\partial t} = div\left(\lambda\,grad\,\vartheta\right) + p_v - \vec{v}\,grad(c\,\rho\,\vartheta) \tag{5}$$

where c is the specific heat, λ is the thermal conductivity coefficient, ρ is the mass density and $\vec{v}$ is the strip velocity.

The computation of the electromagnetic field by approximation is performed on the basis of the 3D FEM with Galerkin method applied to equation (1) and (2). Fig. 1 shows the mesh of

the TFIH equipment and we can easily find two additional planes of symmetry, situated in the middle of the strip (x-y plane) and in the middle of the inductor-yoke combination (y-z plane). So the solution area is reduced to 1/8 of the total volume. In the x-z and the y-z planes of symmetry, the electric current densities are oriented perpendicular to them respectively. Hence on the x-z plane the components of the magnetic vector potential $\vec{\underline{A}}$ and the scalar potential $\underline{\phi}$ are

$$\vec{\underline{A}}_X = \vec{\underline{A}}_Z = 0 \tag{6}$$

$$\frac{\partial \vec{\underline{A}}_Y}{\partial y} = 0 \tag{7}$$

$$\underline{\phi} = 0 \tag{8}$$

And on the y-z plane

$$\vec{\underline{A}}_y = \vec{\underline{A}}_Z = 0 \tag{9}$$

$$\frac{\partial \vec{\underline{A}}_x}{\partial x} = 0 \tag{10}$$

$$\underline{\phi} = 0 \tag{11}$$

On the x-y plane of symmetry, the current density has no perpendicular component and

$$\vec{\underline{A}}_z = 0 \tag{12}$$

$$\frac{\partial \vec{\underline{A}}_x}{\partial x} = \frac{\partial \vec{\underline{A}}_y}{\partial y} = 0 \tag{13}$$

$$\frac{\partial \underline{\phi}}{\partial z} = 0 \tag{14}$$

In this problem, the scalar potential in the electrical non-conductive field areas is practically insignificant, because in the equations (1) and (2) it always appears in conjunction with the electrical conductivity. The perpendicular component of the current density must be zero on the surface of electrical conducting areas, except for the forced source current density. Hence the following equation is valid:

$$j\omega k(\vec{\underline{A}} + grad\underline{\phi}) \cdot \vec{n} = 0 \tag{15}$$

The present problem has an open boundary condition because the vector potential disappears only in the infinity. With the aids of comparative computations, an enveloping surface can, however, be determined for which the condition is valid within a known upper limit of error.

$$\underline{\bar{A}} = 0 \qquad (16)$$

For computation of temperature field, there is no y-z symmetric plane. The heat source density in the newly added area can be obtained by reflection at the y-z plane or by separated computation for a corresponding temperature distribution.

Power losses on the surfaces were taken into account by using non-homogenous Neuman boundary conditions for convection and radiation (17). Where ϑ_s is the surface temperature, ϑ_α is the ambient temperature, α_c is the heat transfer coefficient for convection and α_R is the equivalent heat transfer coefficient for radiation. The calculation of α_R based on the Stefan-Boltzman law and is given by equation (18), where ε is the emissivity coefficient of the surface material and c_R is the radiation number.

$$-\lambda \frac{\partial \vartheta}{\partial n}\bigg|_{\Gamma 3} = \alpha_c (\vartheta_s - \vartheta_\alpha) + \alpha_R (\vartheta_s - \vartheta_\alpha)\big|_{\Gamma_3} \qquad (17)$$

$$\alpha_R = c_R \varepsilon \frac{\left(\dfrac{\vartheta_s + 273}{100}\right)^4 - \left(\dfrac{\vartheta_\alpha + 273}{100}\right)^4}{\vartheta_s - \vartheta_\alpha} \qquad (18)$$

Furthermore, at an adequate distance from the inductor, boundary conditions must be determined over the cross section of the workpiece. On the side from which the strip enters the solution area, temperature (e.g. ambient temperature) is given.

$$\vartheta(x, y, z)\big|_{\Gamma_1} = \vartheta_0(x, y, z)\big|_{\Gamma_1} \qquad (19)$$

On the exit side, however

$$\text{grad } \vartheta \cdot \vec{n} = 0 \qquad (20)$$

is indicated, where $\vec{n}$ corresponds to the velocity direction.

The electromagnetic field and the temperature field are coupled via the temperature dependence of the electrical conductivity and the magnetic permeability. The relationship between eddy current distribution and coil geometry in TFIH equipment was analyzed. The non-linear coupled electromagnetic-thermal problem was solved through finite element method (FEM). Based on that, new coil geometry was designed to get a homogeneous temperature distribution on the surface of the strip, shown in Fig.1 [7].

Fig. 1. New structure of the TFIH equipment

Through the orthogonal experiment above, the more suitable structure can be determined by comparing the distribution of the eddy current and heat source, furthermore that of the temperature on workpiece surface. Fig. 2 gives the distribution of heat sources density computed with equation (4). Fig. 3 shows the temperature distribution resulted from the computation with induced heat sources density shown in Fig. 2.
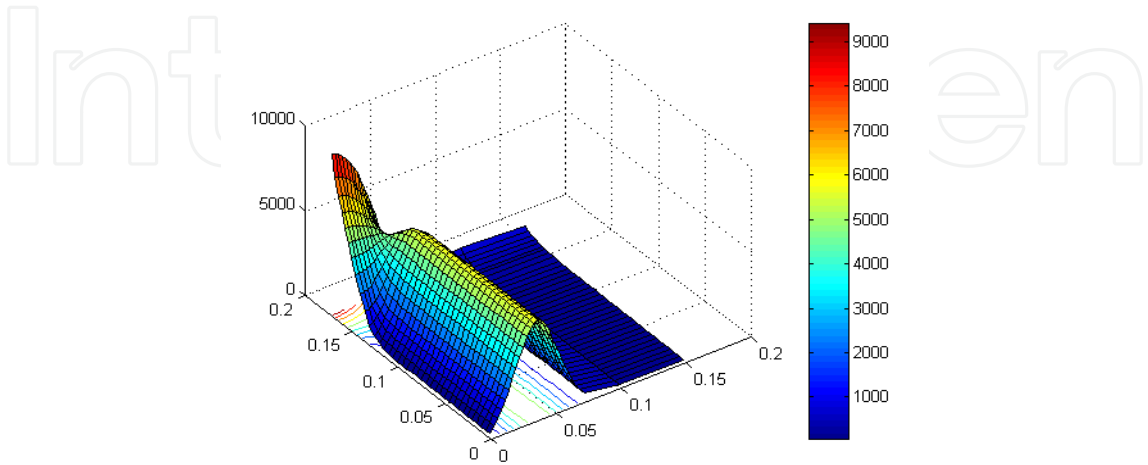
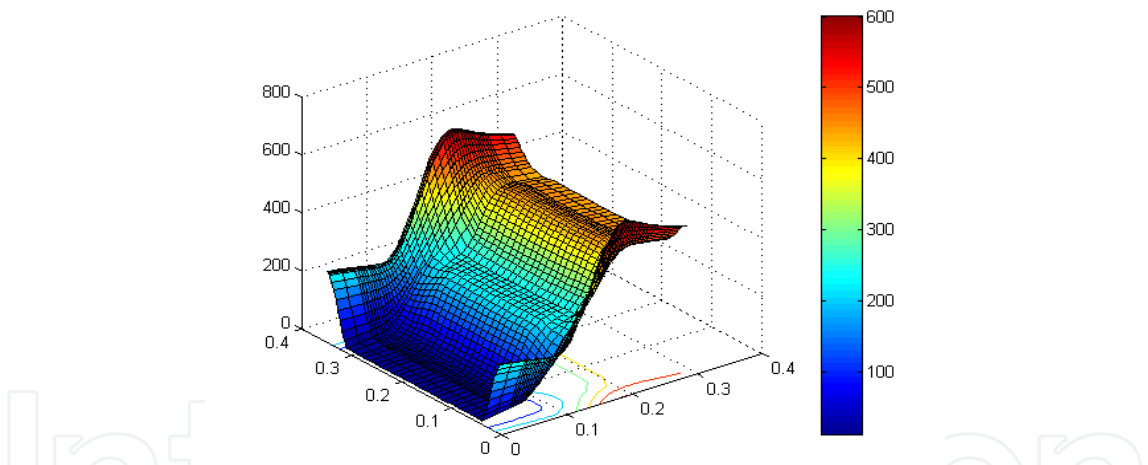Fig. 2. Distribution of heat sources density on the 1/4 surface of the strip

Fig. 3. Temperature distribution on the surface of the strip

In the design of TFIH equipment with orthogonal experiment the computation of eddy current and heat source distributions are beneficial for the optimum chosing of the design parameters in order to obtain a high efficient and homoginous heating across the strip width, the exactly controll of the working process varies from different workpieces by means of the numerical predication model under the industry conditions.

In the case of TFIH, the flux is perpendicular to the surface of the work piece; therefore the eddy current is across the thickness of the work piece. So compared to longitudinal flux induction heating equipments the TFIH equipments have considerable advantages such as a much lower frequency resulting in a higher electrical efficiency, lower reactive power, more suitable for continuously heating treatment and local heating because of its inductor not encircling the work piece.

Neural Networks with FEM was also introduced to predict eddy current and temperature distribution on the continuously moving thin conducting strips in TFIH equipments. With the temperature prediction results, a good guessed value of the temperature dependent parameters for each finite element and initial values for temperature field solution are provided. The predicted results are presented in Fig. 4. Network prediction results speed up the iteratively solution process for the non-linear coupled electromagnetic-thermal problems.
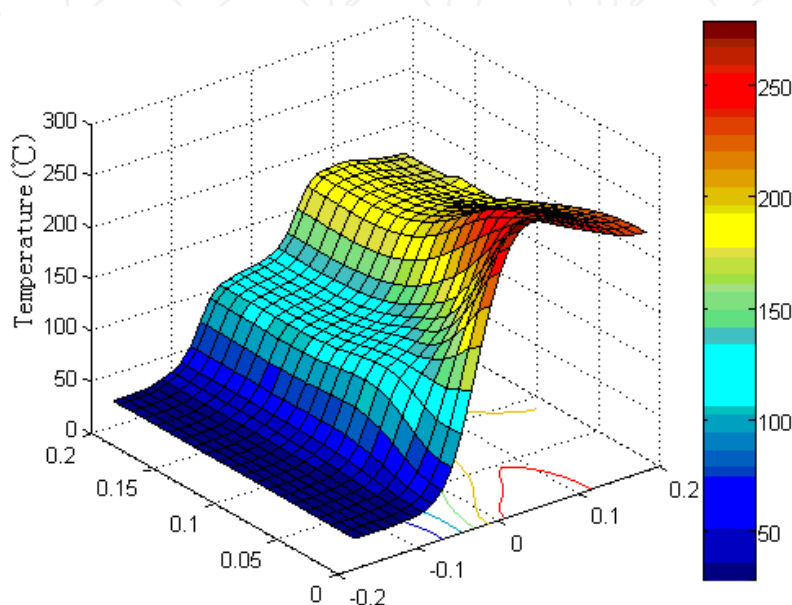
Fig. 4. The predicted result of temperature field distribution on the surface of one half of the thin metal work piece

3. Travelling Wave Induction Heating systems (TWIHs)

Unlike the longitudinal or the single-phase transverse flux heaters, TWIHs is energized with three-phase windings. Parametric analysis is used to assess the key parameters. TWIHs is intrinsically more suitable than its single phase counterpart in the provision of uniform thermal density on the work strips [18]. Indeed, three-phase induction heaters not only have the same advantages as their single-phase counterparts, they can produce more uniform temperature distributions, operate with less industrial noise and vibration. For operations in which the electromagnetic force may increase significantly and the heating parameters could change as the temperature rises, the advantage of TWIHs is even more significant.

3.1 Typical Travelling Wave Induction Heating system (TWIH)

Typical travelling wave induction heating system (TWIH), as one of the multiphase induction heating systems, has particular features which make them attractive for application to some heating and melting processes in industry. Among the advantages we can mention the possibility to heat quite uniformly thin strips or regions of a body without moving the inductor above its surface, to reduce the vibrations of inductor and load due to the electro-dynamic forces and also the noise provoked by them, to obtain nearly balanced distributions of power and temperature [1].

TWIH introduces three-phase induction heating heater, using the typical three-phase windings and parametric analysis to assess the key parameters (transmission of electricity to the work-piece, efficiency, power factor, et al) and the distribution of electricity. Compared with the single-phase induction heating heater of Transverse Flux Induction Heating inductors, three-phase induction heating heater not only has the same advantages, but owns the ability to produce more uniform temperature distributions, and reduces industrial noise with low vibration. Especially in the conditions that electromagnetic force increases significantly and heating parameters change with the rise of temperature, the advantage is very important.

TWIH is of particular interest for theoretical analysis and some industrial applications of induction heating. Since the analysis of bibliography shows that TWIH systems have not been studied so deeply as the single phase ones, the present paper has been devoted to the simulation and study of some peculiar characteristics of this type of inductors. Particular attention has been paid to the simulation of TWIH systems for heating thin strips and plain bodies including TFIH.

Fig. 5 (a) shows the schematic of a typical configuration of the heater with two linear inductors on the opposite sides of the strip, slots perpendicular to the direction of the movement and a relatively large air-gap due to the thickness of the refractory material interposed between the inductor and the strip.
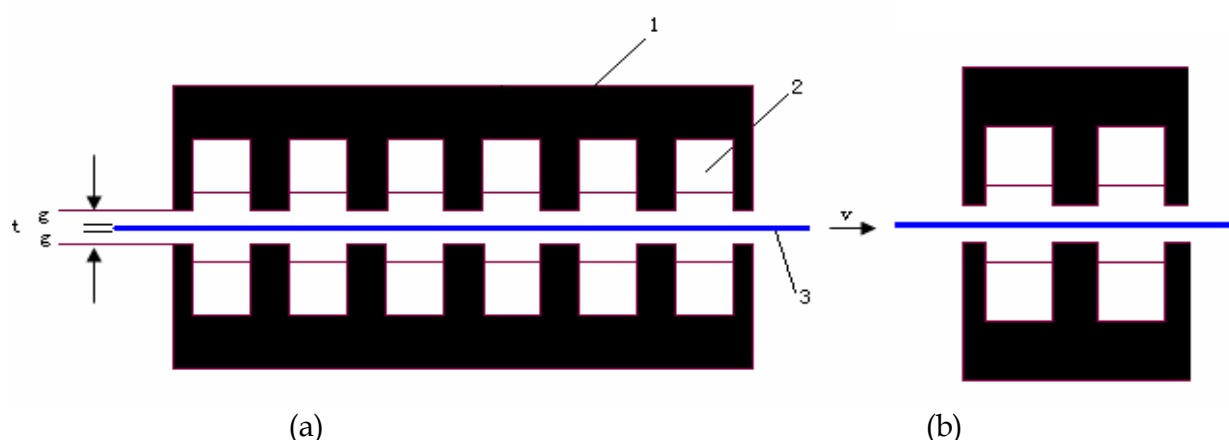

(a)   (b)

Fig. 5. (a) Schematic of a double-side TWIH [1-magnetic yoke; 2-exciting windings; 3-load metal sheet; t-strip thickness; g-airgap between inductor and load; v-strip movement directions]; (b) Schematic of a double-side TFIH.

A schematic of a TFIH system is displayed in Fig. 5 (b). Besides the phases, other parameters are similar to those in TWIH system in Fig. 5. The TFIH inductor configuration analyzed in this chapter has been chosen to be as close as possible to an existing system for assuring the possibility of checking the results by tests.

The TFIH system, shown in Fig. 5 (a), consists of two inductors with current carrying conductors located inside the slots of two magnetic yokes and perpendicular to the length of the strip and to the direction of its movement. The inductors are situated on both sides of the strip [2].

On each inductor there are three coils and six conductors in every coil. The aluminum work-piece has the following dimensions: thickness 2.5 mm, width from 1200 to 1600 mm, while the air gap between magnetic yokes is 60 mm.
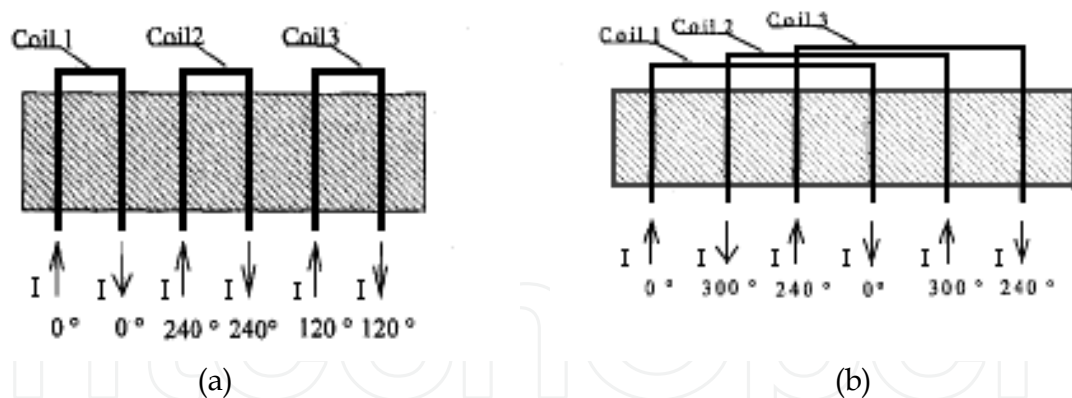
Fig. 6. (a) Coil connections for TFIH; (b) Coil connections for TWIH.

For the purpose of comparison, the same configuration has been used for the TWIH system, but with different schemes of coils connections in order to obtain a travelling wave field, shown in Fig. 6(b). The reference to a similar design for the two systems, which have approximately the same efficiency, gives the possibility of understanding more clearly some basic differences between TFIH and TWIH inductors. As stated before one of the problems. Maxwell equations are the theoretical basis of all macro- electromagnetic phenomena, and its differential equations are as following:

$$\nabla \times \vec{H} = \vec{J} + \frac{\partial \vec{D}}{\partial t} \tag{21}$$

$$\nabla \cdot \vec{B} = 0 \tag{22}$$

$$\nabla \times \vec{E} = -\frac{\partial \vec{B}}{\partial t} \tag{23}$$

$$\nabla \cdot \vec{D} = \rho \tag{24}$$

This project overlooks the functions of the accumulative charges, that is $\rho = 0$. From (21) to (24), $\vec{H}$ -magnetic field intensity, $\vec{J}$ -current density, $\vec{E}$ -electric field intensity, $\vec{B}$ -magnetic field intensity, $\vec{D}$ -electric displacement vector. According to the relationship between $\vec{H}$, $\vec{J}$, $\vec{E}$, $\vec{B}$ and $\vec{D}$, we can get

$$\nabla \times \vec{H} = \vec{J} + \frac{\partial \vec{D}}{\partial t} = \sigma \vec{E} + \frac{\partial}{\partial t}(\varepsilon \vec{E}) \tag{25}$$

The corresponding vector form

$$\nabla \times \tilde{\vec{H}} = (\sigma + j\varepsilon\omega)\tilde{\vec{E}} \tag{26}$$

When $\sigma >> \varepsilon\omega$, $\frac{\partial \vec{D}}{\partial t}$ can be neglected. And when the frequency is up to thousands of hertz, it satisfies $\sigma >> \varepsilon\omega$. Therefore, in this project we can neglect $\frac{\partial \vec{D}}{\partial t}$. Equation (21) is simplified as

$$\nabla \times \vec{H} = \vec{J} \tag{27}$$

For the eddy current field, basic equations can be established with $\vec{A} - \phi$ method. Then we introduce magnetic vector potential $\vec{A}$, define it as $\vec{B} = \nabla \times \vec{A}$, and eventually attain the current density formula

$$\vec{J} = -\sigma(\frac{\partial \vec{A}}{\partial t} + \nabla \frac{\partial \phi}{\partial t}) + \vec{J}_s \tag{28}$$

TFIH and TWIH comply with the Maxwell equations strictly in theory. From the equations above we can see that the current density in the strip is decided by the magnetic flux and the field intensity, so magnetic field inducted by TFIH and TWIH can create different vortex effect in the strip.

Both analytical and numerical techniques can be used for the study of these heating systems. Analytical methods are more convenient for the integral parameters determination and analysis, while the numerical techniques are more universal and particularly useful for investigating the induced current and power distributions, taking into account the inductor edge-effects and the slots effects which are usually well pronounced in TWIH systems. The analytical methods which make use of Fourier integral transformation or series are effective for the simulation of lD, 2D and even 3D multiphase devices, but some simplifications and assumptions must be made.

Recently some dedicated analytical codes, described in previous papers, have been developed by the authors and applied to the study of such systems [3, 6, 8, 9]. However, they introduce in the simulation some rough simplifying assumptions (e.g. current sheet inductors, yoke without slots) which, for some purposes, are too far from reality. On the other hand, numerical methods are more universal and able to solve problems for more complex geometries. Their use is practically mandatory when the tooth pulsation, the influence of the slot-tooth ratio and slot depth or the inductor and load edge effects have to be taken into account.

Since in this chapter the influence of the relative slot-tooth position of the upper and lower inductor has to be considered, the analysis has been performed by 2D FEM code, overcoming many of the above difficulties by the use of a specially built computer programmer in which the FEM code is called as an external subroutine [10, 11]. Given the system geometry, the programmer automatically performs with the changes of the geometrical and electrical data, without the direct intervenes of the FEM code users. In order to study the efficiency of TWIH system, the magnetic flux density distribution is calculated. It is displayed in Fig. 7. (Current density is 3 A/mm², and frequency is 600 Hz).

TFIH system magnetic induction intensity distributes symmetrically along both sides of axis and reach the top above magnetic yokes, and the intensity is relatively weak above the coils. Near the center of axis the intensity decreases to the minimum. The curve of TWIH system's magnetic flux density in Fig. 7 (a) is relatively more homogeneous than TFIH heater's which shows low degree only between 130 mm and 175 mm region.

Fig. 8 show results about eddy current density distributions in TFIH and TWIH systems. As TWIH using three-phase induction heaters, upper and lower induction heaters can be installed properly to make up better for the low-fields, so as to achieve uniform heating results.
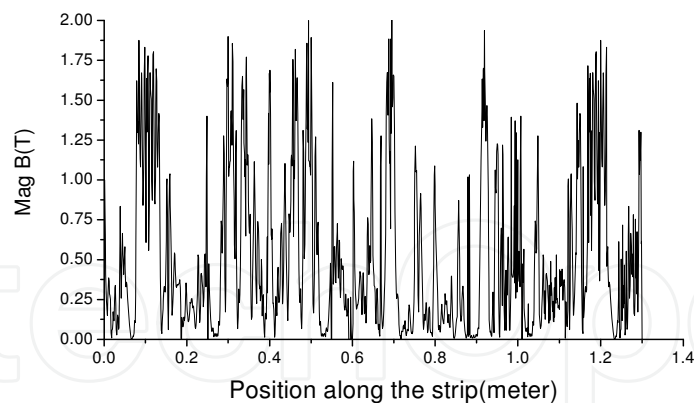
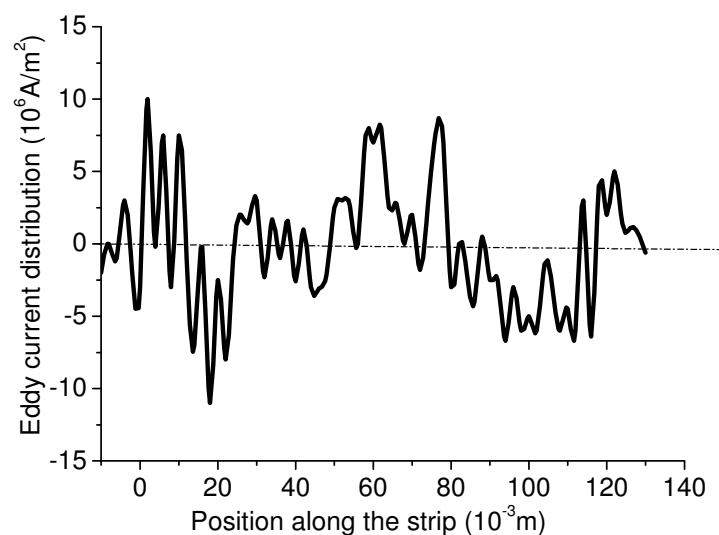Fig. 7. The magnetic flux density distribution in the strip of TWIH system at 600Hz.

Fig. 8. The eddy current density distribution along the strip perpendicularly of TWIH system at 600Hz

Another characteristic of the TFIH system here considered is the presence of many high eddy current peaks along the direction of the movement along the edge of the sheet, which can give rise to, in some cases, dangerous strip deformations. In the corresponding TWIH system this problem is reduced since few and less sharp peaks with their highest value much less than in TFIH system are present. The same situation arises in centre of the sheet, but due to the very similar configuration of TWIH and TFIH inductors, in both systems eddy current peaks are present.

3.2 Crossed traveling wave induction heating (C-TWIH)

A novel design for a crossed traveling wave induction heating (C-TWIH) system is proposed to address the inhomogeneous eddy current density which dominates the temperature distribution on the surface of work strips. FEM is used to calculate the eddy current and temperature distributions. Simulation results of the novel C-TWIH system are presented and compared with those of typical TWIH and TFIH systems to showcase its better performance.

The schematic of a typical heater configuration is shown in Fig. 9 (a). There are two linear inductors on the opposite sides of the strip and twelve slots along the direction of the movement. There is a relatively large airgap between the inductor and the strip due to the thickness of the interposing refractory materials.
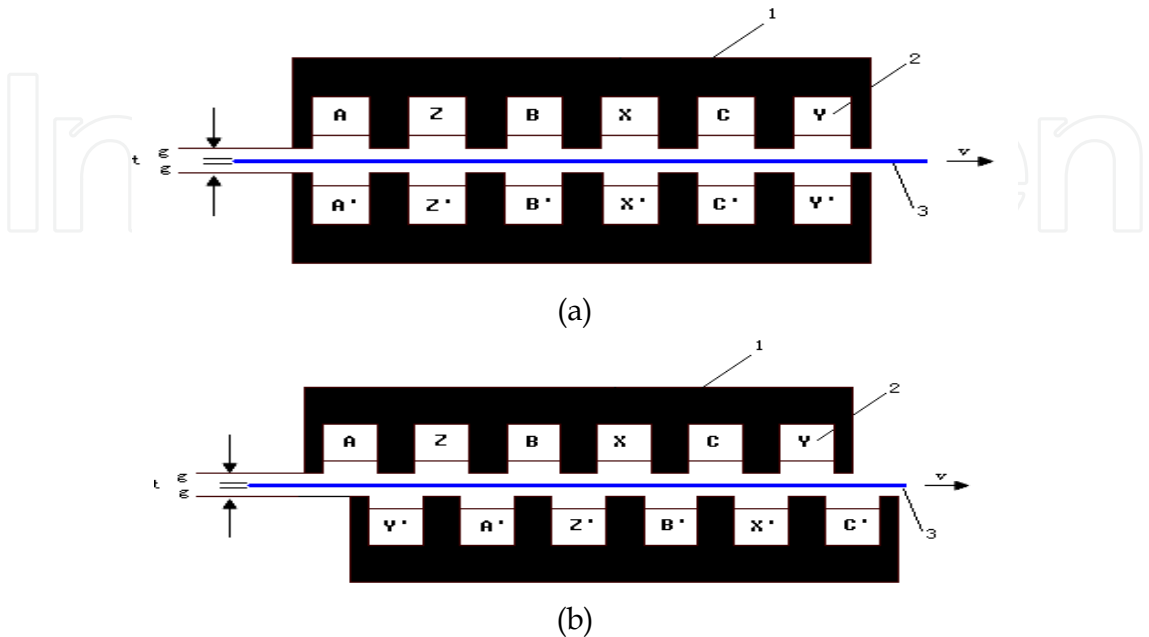

(a)

(b)

Fig. 9. (a) Schematic of a typical double-sided TWIH system; (b) Schematic of the double-sided C-TWIH system (1-magnetic yoke; 2-exciting windings; 3-load metal sheet; *t*-strip thickness; *g*-airgap between inductor and load; *v*-strip movement velocity. Phase degree: *A-X* and *A'-X'*=0º, *B-Y* and *B'-Y'* =-120 º, *C-Z* and *C'-Z'* =-240 º).

The proposed C-TWIH system is shown in Fig. 9 (b). With this structure the lower inductor is shifted 60 degrees along the movement direction of the strip and the winding starts from phase Y'. On each inductor there are three phases and six windings. Alternating current through every two in-phase sets of windings sets up the magnetic field, which is perpendicular to the surface of the sheet, and eddy currents are induced by the alternating magnetic flux on the work strip.

Number of phases	3
Number of windings	6
Number of slots	12
Airgap distance (*g*)	1.0 mm
Magnetic yoke length	1300mm
Magnetic yoke height	200mm
Aluminum strip width	130 mm
Aluminum strip thickness (*t*)	2.0 mm
Strip movement velocity (*v*)	1.0 m/min

Table I. Design Data of Typical TWIH and C-TWIH Heaters of Fig. 1

In the following FEM simulation, the amplitude of the exciting current is 1200A at 600Hz. The phase current waveforms are as shown in Fig. 10. It can be seen from Figs. 10 and 11 that at any instant, there are always four inductor phase windings acting as the field windings to generate the flux in the C-TWIH device; while in typical TWIH device, there are two phase windings only.
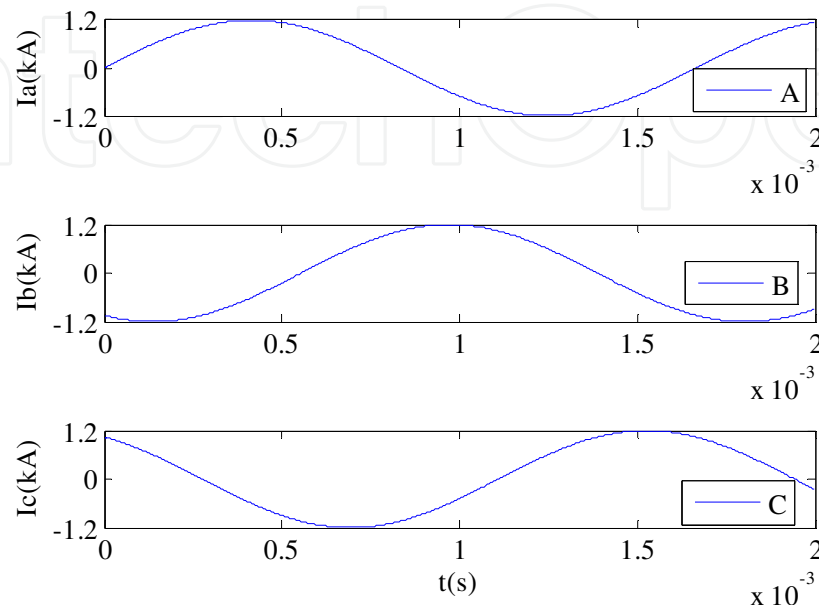

Fig. 10. Three-phase exciting current waveforms for typical TWIH and C-TWIH systems

In this section, the operation of the two three-phase induction heating devices, namely the typical TWIH and C-TWIH, with the phase currents of Fig. 10 are investigated using FEM analysis. Particular attention is paid to the analysis of the magnetic flux density, eddy current distribution, power density and the temperature field.

Because AC current through every winding generates a magnetic field, which induces eddy currents to produce the thermal field, the total magnetic field is the additive contribution of six upper-and-lower windings.

$$\oint H dl = \sum i = N_c i \qquad 29)$$

where N_c is the number of turns per phase per winding, and

$$i = \sqrt{2} I \sin(\omega t + \theta) \qquad (30)$$

where I is the r.m.s. current and θ is the phase angle.

The result of the airgap flux density calculation of the C-TWIH system is shown at different positions in Fig. 11. The average trend of the airgap flux density B has a symmetrical waveform having similarly triangle-topped amplitude. Flux densities in the upper and lower inductors make up for the weak areas of each other. This leads to a more uniform eddy current density in the work strips, as discussed below.

The magnetic flux densities in the work strip of the C-TWIH system are depicted in Fig. 12 (b). In order to study the efficiency of the C-TWIH system, the flux density distribution along the work strips of a typical TWIH system is also calculated, which is shown in Fig. 12 (a).
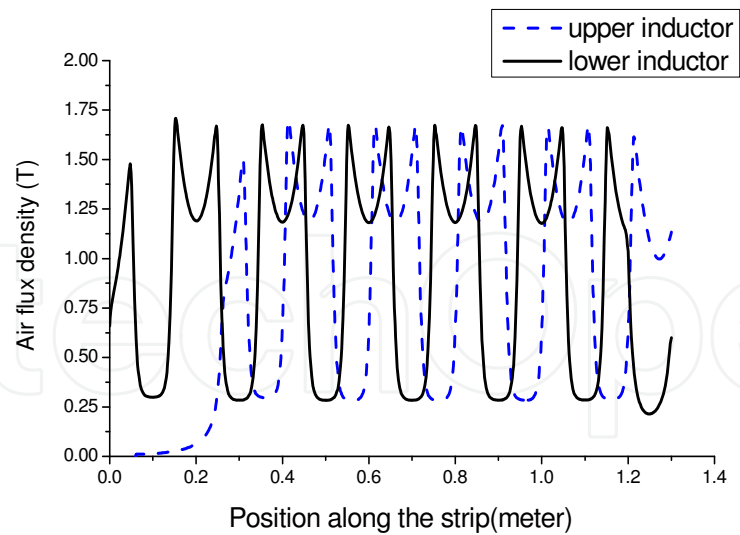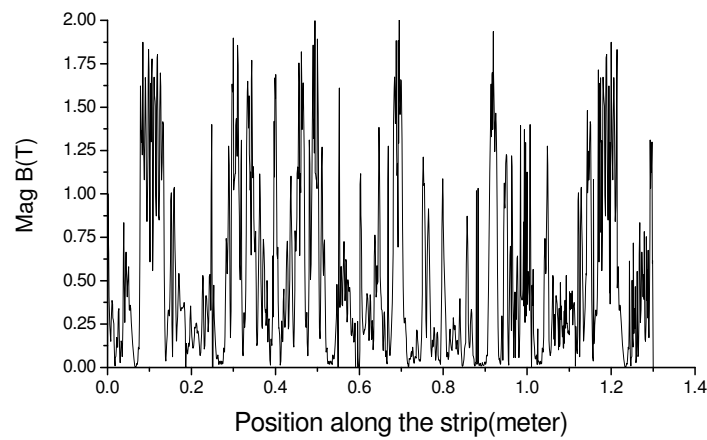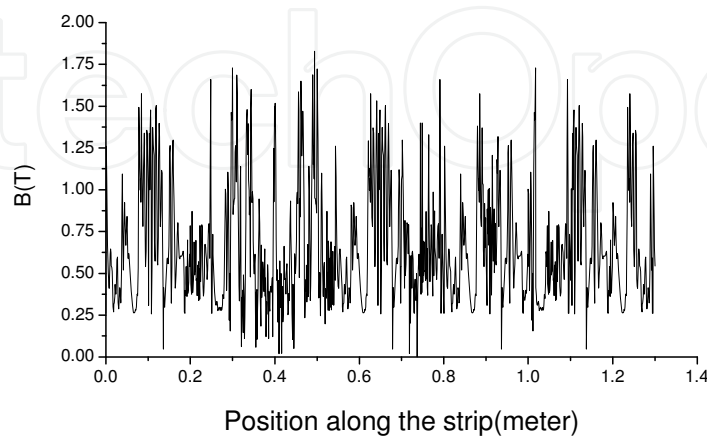
Fig. 11. The airgap flux density distribution in the work strip from the upper and lower inductors

(a) In typical TWIH system

(b) In C-TWIH system

Fig. 12. The magnetic flux density distribution in the work strip.

It can be seen that typical TWIH system's magnetic flux is distributed symmetrically along both sides of the axis and reaches the maximum above the magnetic yokes, while the magnetic flux intensity is relatively weak above the windings. Near the center of axis the intensity decreases to the minimum. The curve of the C-TWIH system's magnetic flux density is relatively more homogeneous than that of typical TWIH heater, which shows low density only in several limited regions. Thus the eddy current field and the temperature field distributions on the work strip should be more uniform in the proposed C-TWIH system than that in typical TWIH systems as confirmed below.

For the induced eddy current field, the basic equations are established using $\vec{A} - \phi$ formulation. The magnetic vector potential $\vec{A}$ is defined as $\vec{B} = \nabla \times \vec{A}$ and the current density is

$$\vec{J} = -\sigma(\frac{\partial \vec{A}}{\partial t} + \nabla \varphi) + \vec{J}_s \tag{31}$$

where σ is the electric conductivity; $\vec{J}_s$ is the impressed exciting current density; $\vec{E}$ is the electric field intensity; and

$$\nabla \varphi = -\vec{E} \tag{32}$$

The induced current density in the strip is generated by variations in the magnetic flux. The vortex effects in the strip are attributed to the magnetic fields produced by different structures of typical TWIHs or other types of heaters like TFIH. By using FEM, the magnetic flux distributions and induced eddy current density in the strip of typical TWIH and C-TWIH systems are shown, respectively, in Figs. 13 (a) and (b) for electrical phase angles of 90° and 270°.

It is shown in Fig. 13 that the novel C-TWIH system has a relatively more uniform power density distribution. This is accomplished mainly because of the application of crossed three-phase AC excitations to create uniform magnetic fields that govern the eddy current density distribution. On the other hand, the combination of six induction heaters serves to widen the directions of the induced magnetic field which is distributed along the magnetic yokes. These inductors interact with each other and compensate for the weak magnetic areas existing between the gap districts.

Fig. 14 shows the eddy current density distributions in typical TWIH and C-TWIH systems. As C-TWIH uses crossed three-phase induction heaters, the upper and lower induction heaters are installed properly to compensate for the low-fields so as to realize uniform heating results. It can be seen that the eddy current distributions are more uniform in C-TWIH when compared to those in typical TWIH.

Another characteristic of TWIH systems that needs to be considered is the presence of many high eddy current peaks along the movement directions on the edges of the sheet, which can give rise to, in some cases, dangerous strip deformations. In the proposed C-TWIH system this problem is reduced since sharp peaks of eddy currents are much fewer than those in typical TWIH systems.

The best cases among both typical TWIH and C-TWIH system [12], which has the similar geometry, are compared in Fig. 15, where the irregularities due to the use of a relatively small number of mesh elements have been smoothed. It can be seen that from 3 mm to 130 mm, the C-TWIH system induces higher power than any other systems being studied.

Phase degree: 90°   Phase degree: 270°

(a) Typical TWIH

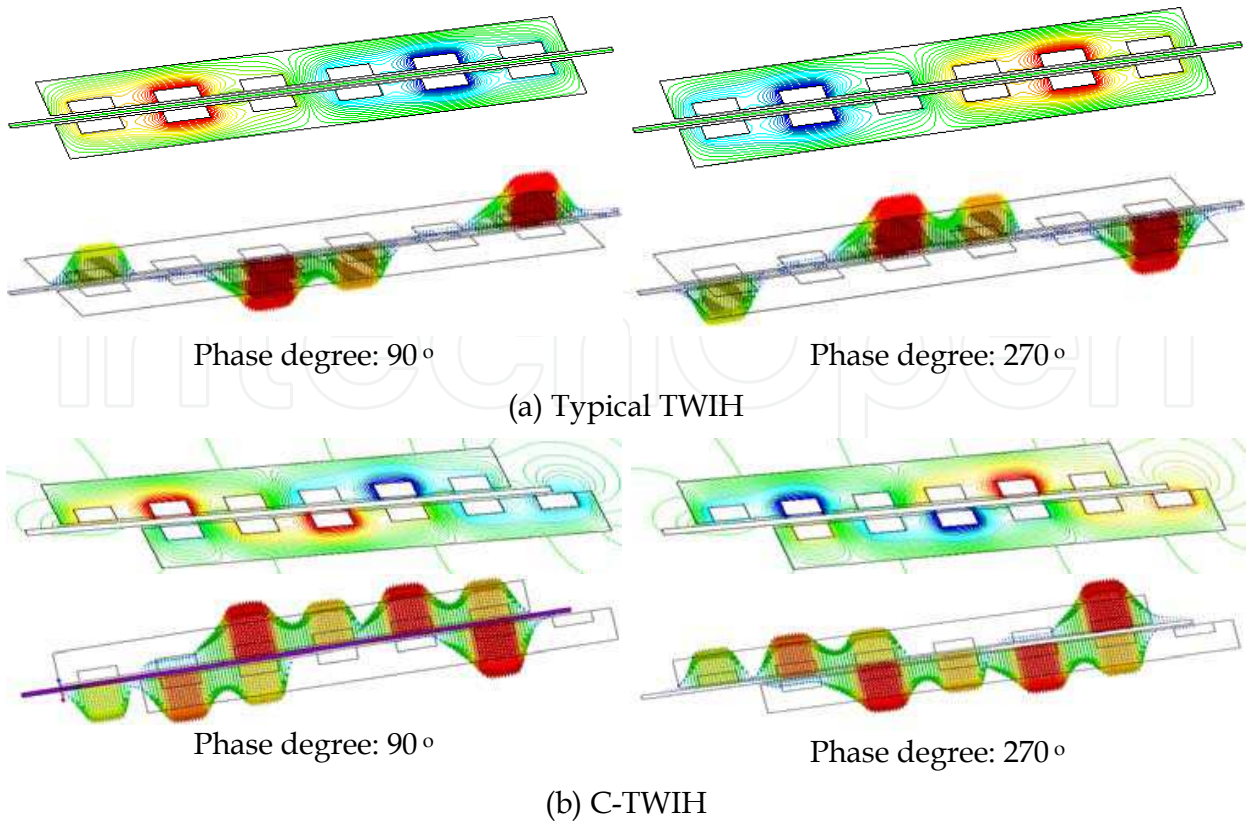Phase degree: 90°   Phase degree: 270°

(b) C-TWIH

Fig. 13. Magnetic flux distributions in the strip and induced power density distributions along the direction of the strip movement (yoke size - 1300×30mm; slot size - 150 ×50 mm; airgap - 1 mm; strip thickness - 2 mm; currents supply I –1200A; f - 600 Hz).
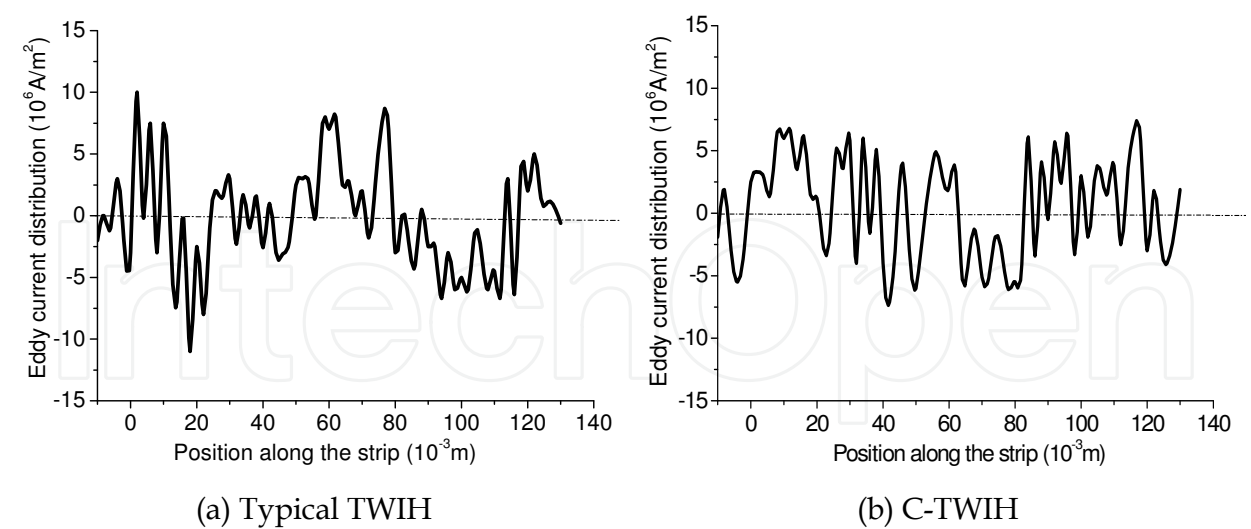

(a) Typical TWIH   (b) C-TWIH

Fig. 14. The eddy current density distribution along the strip perpendicularly of typical TWIH and C-TWIH systems

The thermal properties of the materials are functions of temperature. Around the surface of the heating regions, there are dramatic changes in the high temperature zones. In order to improve the accuracy of the simulation, 2D nonlinear transient heat conduction equations are introduced to describe the thermal fields.
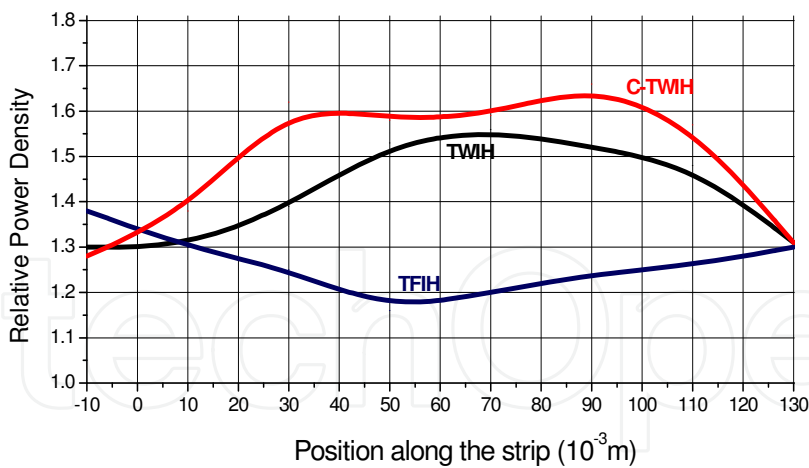
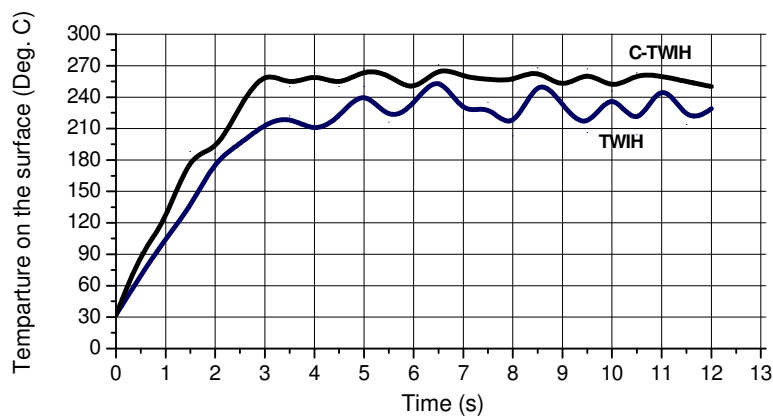Fig. 15. Relative Power density (P_2/P_1) distribution of C-TWIH, TWIH and TFIH

Fig. 16. Temperature distribution along the surface of the strip

Applying eddy current density to be the heat sources during the heating process, the thermal source is

$$P_V = \frac{\left|\bar{J}\right|^2}{\sigma} \tag{33}$$

where $\bar{J}$ is the eddy current density and σ is the electric conductivity.

The temperature field is computed based on Fourier's thermal conduction equation

$$\frac{\partial(c\rho\vartheta)}{\partial t} = \nabla \cdot (\lambda\nabla\vartheta) + P_V + \bar{v} \cdot (c\rho\vartheta) \tag{34}$$

where c is the specific heat; ρ is the mass density; λ is the thermal conductivity coefficient; P_V is the thermal source; and $\bar{v}$ is the strip velocity.

Fig. 16 shows that the C-TWIH reaches a higher temperature faster and with fewer variations when compared to typical TWIH. After three seconds, the temperature of typical TWIH is observed to fluctuate between 212°C and 256°C, while C-TWIH has a temperature range from 251°C to 270°C and its unexpected temperature difference is reduced by about 43% compared to that in typical TWIH device.

In addition, the proposed C-TWIH system can overcome problems of metal deformation and reduces the noise from the system, where the uniformity of power and eddy currents in the work strips plays an important role.

3.3 Traveling wave induction heating system with distributed windings and magnetic slot wedges (SW-TWIH)

A traveling wave induction heating system with distributed windings and magnetic slot wedges (SW-TWIH) and its improved system are proposed to address the inhomogeneous eddy-current density that dominates the temperature distribution on the surface of work strip. Magnetic flux distributions and eddy current distributions are computed using FEM. Performance of the novel SW-TWIH and an improved version is also presented and compared with a typical TWIH [6, 13, 14] using FEM to showcase the merits of the proposed system.
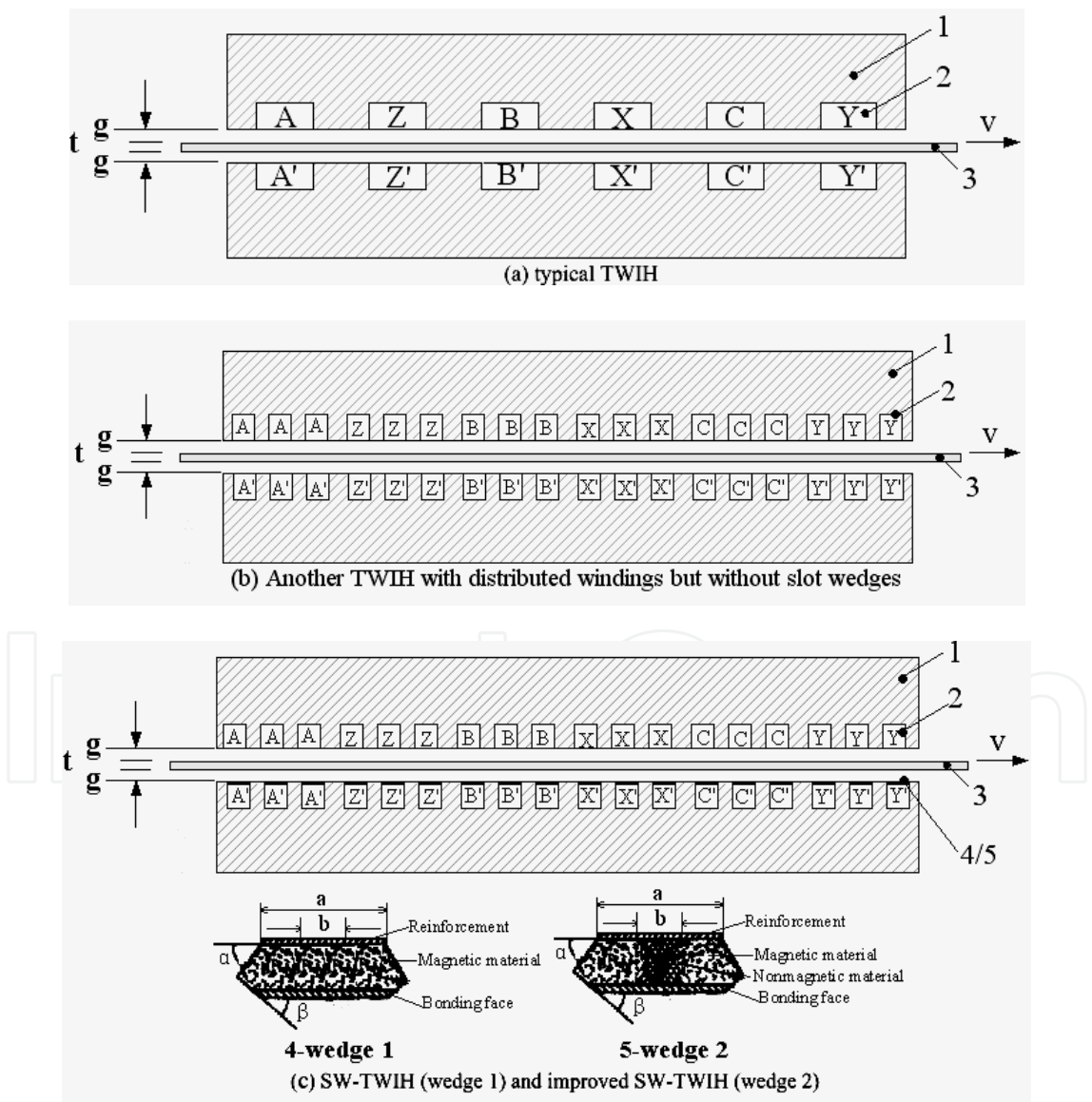
Fig. 17. Schematics of the systems.

Similar to the study of traditional longitudinal heaters, two-axis equivalent circuit method is usually employed in the steady-state performance study of TWIH [3]. For transient performance, such as eddy current and temperature field distributions, the results from traditional methods are not as accurate as expected, due to skin effects on the solid pole surface and serious magnetic nonlinearities. With the advent of powerful computing workstations, 2D and 3D finite-element analyses (FEAs) have now become feasible in practical applications, not only for steady-state field analysis, but also for transient performance study of induction heaters [1, 6, 11, 13]. For complicated TWIHs, transient 3D FEA study to include the eddy current and temperature field distributions is however computationally expensive and are hence not feasible for industrial applications due to its complex 3D meshing process and excessively long solution time required.

In order to study the performance of the proposed SW-TWIH system, an interpolative FEA modeling method is introduced [15]. The salient performance of the proposed SW-TWIH device can then be obtained accurately using a 2D transient FEA simulation.

Fig. 17 (a) is a typical TWIH system and Fig. 17 (b) represents the TWIH system with distributed windings but without slot wedges. The proposed SW-TWIH system is shown in Fig. 17 (c), which has the same structure but with magnetic slot wedges (SW) in each coil. Two linear inductors and thirty three coils are equipped on the opposite sides of the strip along the direction of movement. Due to the thickness of the interposing refractory materials, there is a relatively large airgap between the inductor and the strip. For the improved system, a nonmagnetic strip is equipped in the middle of SW. Table II gives the parameters of the proposed system.

For the transient analysis, the time step needs to be sufficiently fine, such as 0.01 ms in this study, so as to simulate the eddy current distribution correctly. Based on the observations, it is estimated that it takes more than a few days in order to obtain the complete solution with 3D FEA. Such a long computation period is impractical for engineering applications.

	Number of phases	3
	Number of windings	6
	Number of slots	36
	Airgap distance (g)	1.0 mm
The proposed heater	Magnetic yoke length	1400 mm
	Magnetic yoke height	120 mm
	Slot width	33.3 mm
	Slot height	60 mm
Width of aluminum strip		130 mm
Thickness of aluminum strip (t)		3.0 mm
Movement velocity of strip (v)		1.0 m/min
The width of nonmagnetic material in improved SW-TWIH system		2 mm

Table II. Design Data of The Proposed Heaters

Two main causes that contribute to inaccurate simulation results when using 2D models are the end-turn leakage inductance and the equivalent effective core length as 3D simulations

are needed. A 2D transient FEA model with the above parameters from 3-D FEA is proposed in this study and the end-turn leakage inductance and effective core length are computed according to the method mentioned in [15].

The operation of the novel 3-phase induction heating devices, namely the SW-TWIH system, and its improved system are investigated using FEM with phase currents as given in Table II. The amplitude of the exciting current is 1200A at 500Hz. The winding current phases of W1, W2, and W3 are 0°, -120°, and -240°, respectively, for the equivalent 2-D transient FEA model. Particular attention is paid to the analysis of the magnetic flux density in the airgap, the eddy current distribution, and the power density.

For the magnetic flux density field, the basic equations are established using $\bar{T} - \Omega$ formulation. $\bar{T}$ is the magnetic vector potential and Ω is the magnetic scalar potential. Applying Ampere's law, Faraday's law, and Gauss's law for the solenoidality of the flux density yields the differential equations in conducting region as

$$\nabla \times \left(\frac{1}{\sigma} \nabla \times \bar{T} \right) + \frac{d}{dt} \left(\mu \bar{T} + \mu \nabla \Omega \right) = -\frac{d}{dt} \left(\mu \bar{H}_S \right) \tag{35}$$

$$\nabla \cdot \left(\mu \bar{T} + \mu \nabla \Omega \right) = -\nabla \cdot \left(\mu \bar{H}_S \right) \tag{36}$$

where $\bar{H}_S$ is a source field; σ is the electric conductivity; and μ is the relative permeability.

Because AC current through every winding generates a magnetic field, which induces eddy currents to produce the thermal field, the total magnetic field is the additive contribution of six pairs of upper-and-lower windings.

Results of the airgap flux densities of the typical TWIH, the TWIH system with distributed windings but without slot wedges, the proposed SW-TWIH and the improved SW-TWIH system are shown in Fig. 18. In the typical TWIH system, the average trend of the airgap flux density B has a symmetrical waveform having similarly triangular-topped amplitudes and large peaks. After applying the distributed windings without slot wedges, the airgap flux density becomes larger and more uniform but also has large differences between the flux peaks. For SW-TWIH system and its improved partner, the weak areas of the flux densities between two neighboring coil slots in the inductors are compensated due to the magnetic SW, which makes the whole flux density distribution more uniform. And compared to SW-TWIH, the improved SW-TWIH system also provides higher flux density because of the nonmagnetic strip in the SW. In fact, the curve of the improved SW-TWIH system's magnetic flux density is relatively more homogeneous than those of others, which shows low density only in several limited regions. Thus the eddy current field and then the temperature field distributions on the work strip should be more uniform in the improved SW-TWIH system than those in other systems mentioned earlier as discussed and confirmed below.

The relationship between eddy current density $\bar{J}_S$ and the source field $\bar{H}_S$ is deduced by Maxwell electromagnetic equations as

$$\nabla \left(\nabla \cdot \bar{H}_S \right) - \mu \sigma \frac{\partial \bar{H}_S}{\partial t} = \nabla \times \bar{J}_S \tag{37}$$
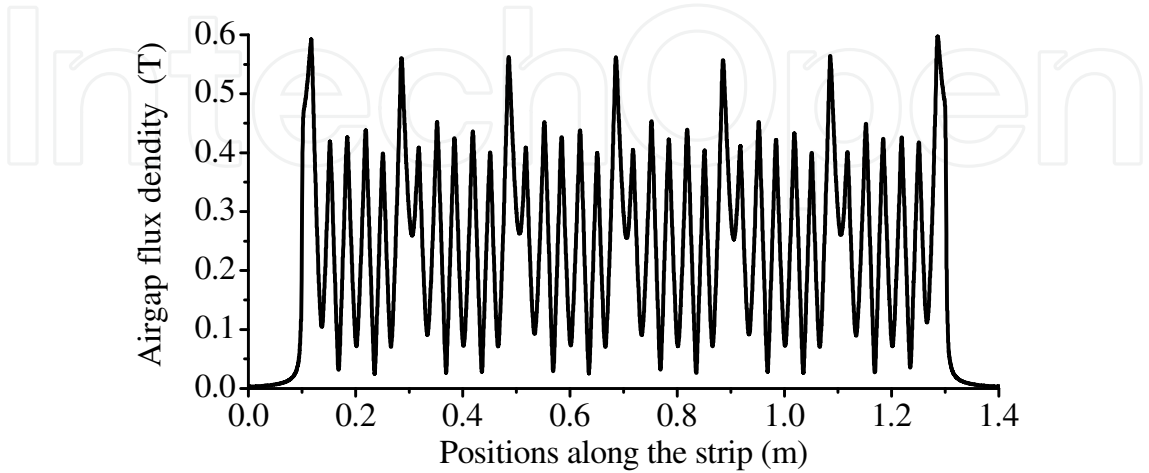
The induced current density in the strip is generated by variations in the magnetic flux. The vortex effects in the strips are attributed to the magnetic fields produced by different structures of TWIHs or other types of heaters like TFIH devices.
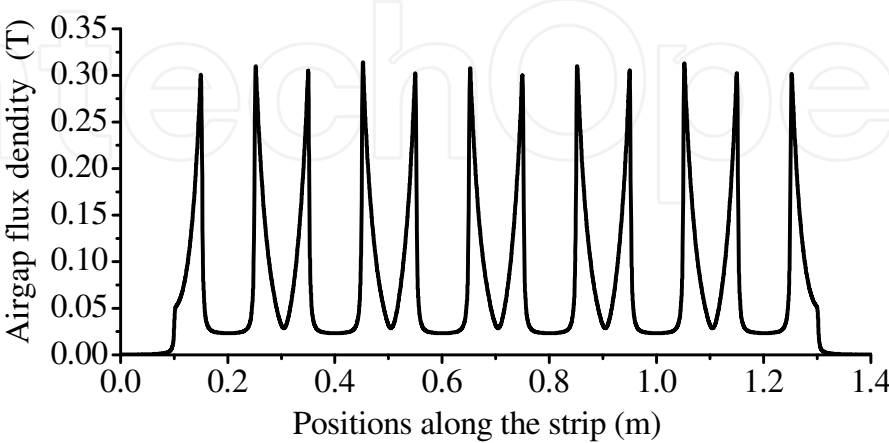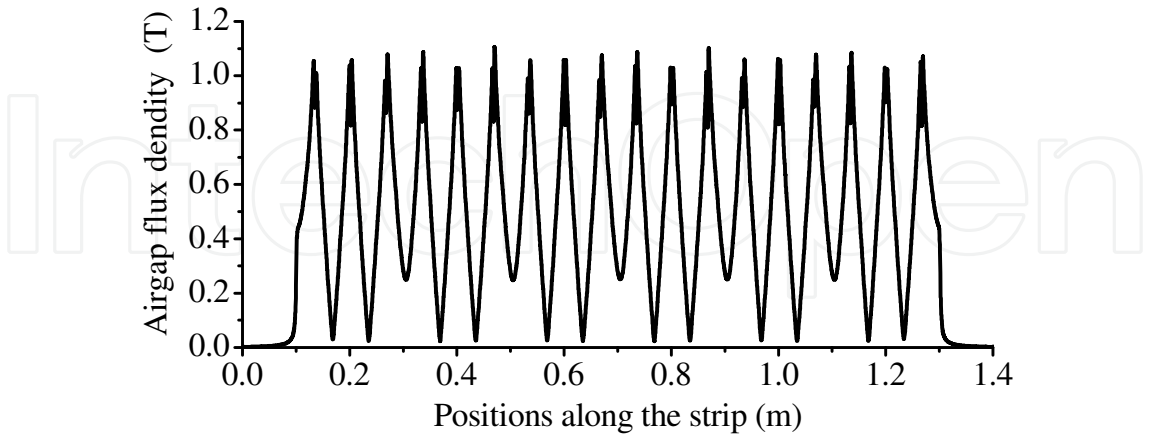
(a) Typical TWIH system
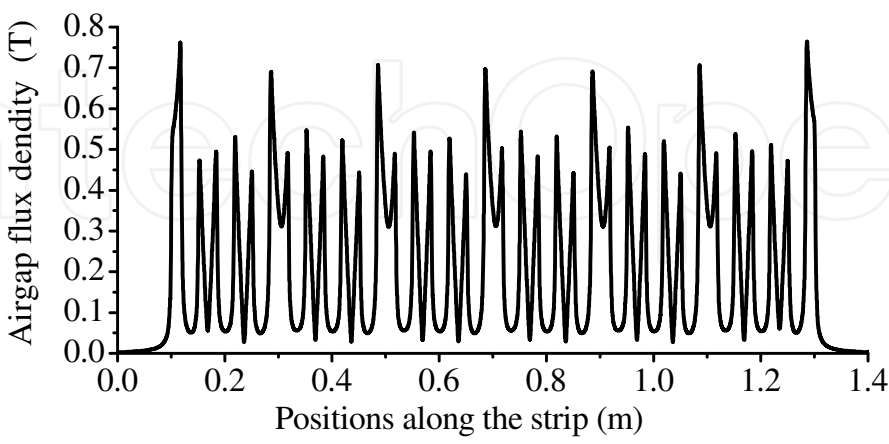
(b) TWIH system with distributed windings but without slot wedges

(c) Proposed SW-TWIH

(d) Improved SW-TWIH system

Fig. 18. The airgap flux density distribution along the direction of the strip movement.

By using FEM, the magnetic flux distributions of the improved SW-TWIH system are shown in Figs. 29 at the phase of 0°, 90°, 180°, 270° and 360°. It can be seen in Fig. 20 that the novel improved SW-TWIH system has a relatively more uniform magnetic flux density distribution. This is accomplished mainly because of the application of three-phase AC excitations to create uniform magnetic fields that largely govern the eddy-current density distribution. On the other hand, the combination of distributed windings and SWs serves to widen the directions of the induced magnetic field which is distributed along the magnetic yokes. These factors interact with each other and compensate for the weak magnetic areas that exist between the gap districts.

Fig. 20 shows the eddy-current density distributions in typical TWIH, the proposed SW-TWIH and the improved SW-TWIH system. It can be seen that the eddy-current distributions are more uniform in the two proposed systems, especially in the improved SW-TWIH, when compared to those in typical TWIH system because of the application of the distributed windings and the magnetic SWs. Also, the combination of six induction heaters serves to widen the directions of the induced magnetic fields along the magnetic yokes. For the improved SW-TWIH system, the nonmagnetic material strip decreases the magnetic flux leakage to result in a relatively higher magnetic flux density.

Another characteristic of typical TWIH system that needs to be considered is the presence of many high eddy-current peaks along the movement directions on the edges of the sheet, which can give rise to, in some cases, dangerous strip deformations. In the proposed SW-TWIH system and its improved partner, this problem is reduced since sharp peaks of eddy currents are much fewer. The eddy current mean square deviations are 18.7303 for the typical TWIH being studied, 8.606 for the SW-TWIH and 11.731 for the improved SW-TWIH, respectively.

The best cases among the typical TWIH, the proposed SW-TWIH and the improved SW-TWIH system are compared in Fig. 21, where the irregularities due to the use of a relatively

(a) At 0 Deg. Phase

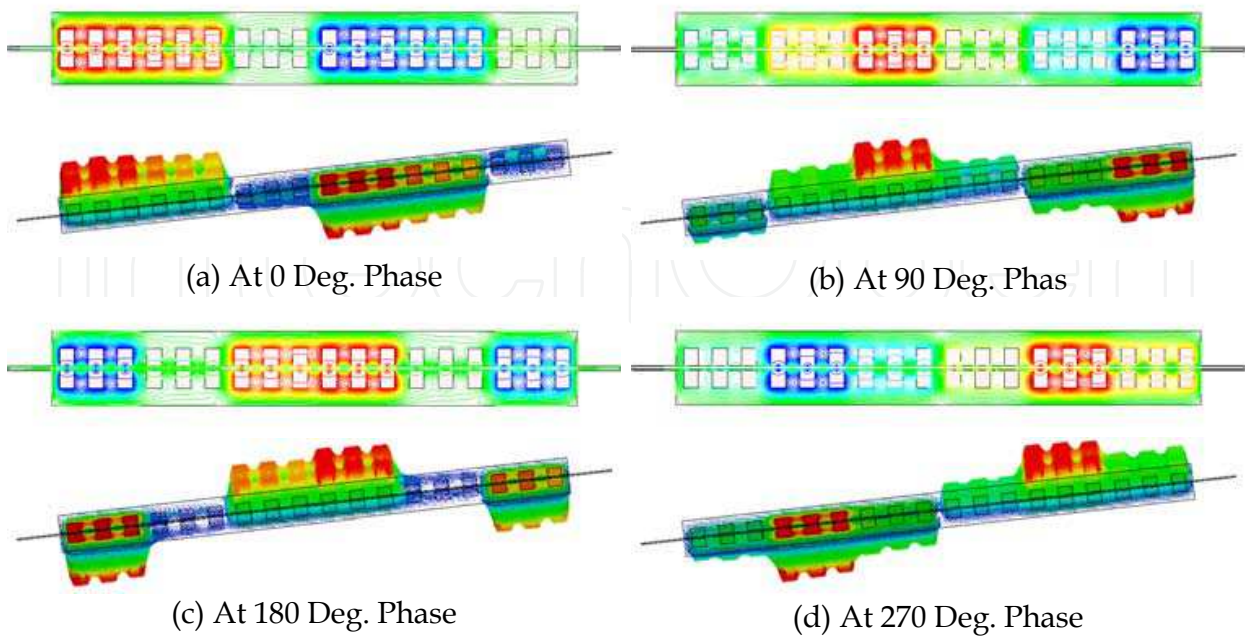(b) At 90 Deg. Phas

(c) At 180 Deg. Phase

(d) At 270 Deg. Phase

Fig. 19. Magnetic flux distributions of the improved SW-TWIH system along the direction of the strip movement.

small number of mesh elements have been smoothened. It can be seen that from 0.16 m to 1.32 m, the SW-TWIH and improved SW-TWIH systems, particularly the latter, produce more uniform power density than that in the typical TWIH system being studied. The improved SW-TWIH system also attains nearly double power density distributions comparing to the other two systems. Therefore, the improved SW-TWIH system provides relatively more homogeneous power distributions and much larger power supply.

For the improved SW-TWIH, the power factor changes with the airgap width of the nonmagnetic material in the magnetic slot wedges, and Fig. 22 shows the trend. The power factor becomes higher when the width is increased, but the distribution uniformity becomes worse according to the analysis. Hence it is essential to select a compromise value based on practical requirements in order to balance uniformity and power factor.
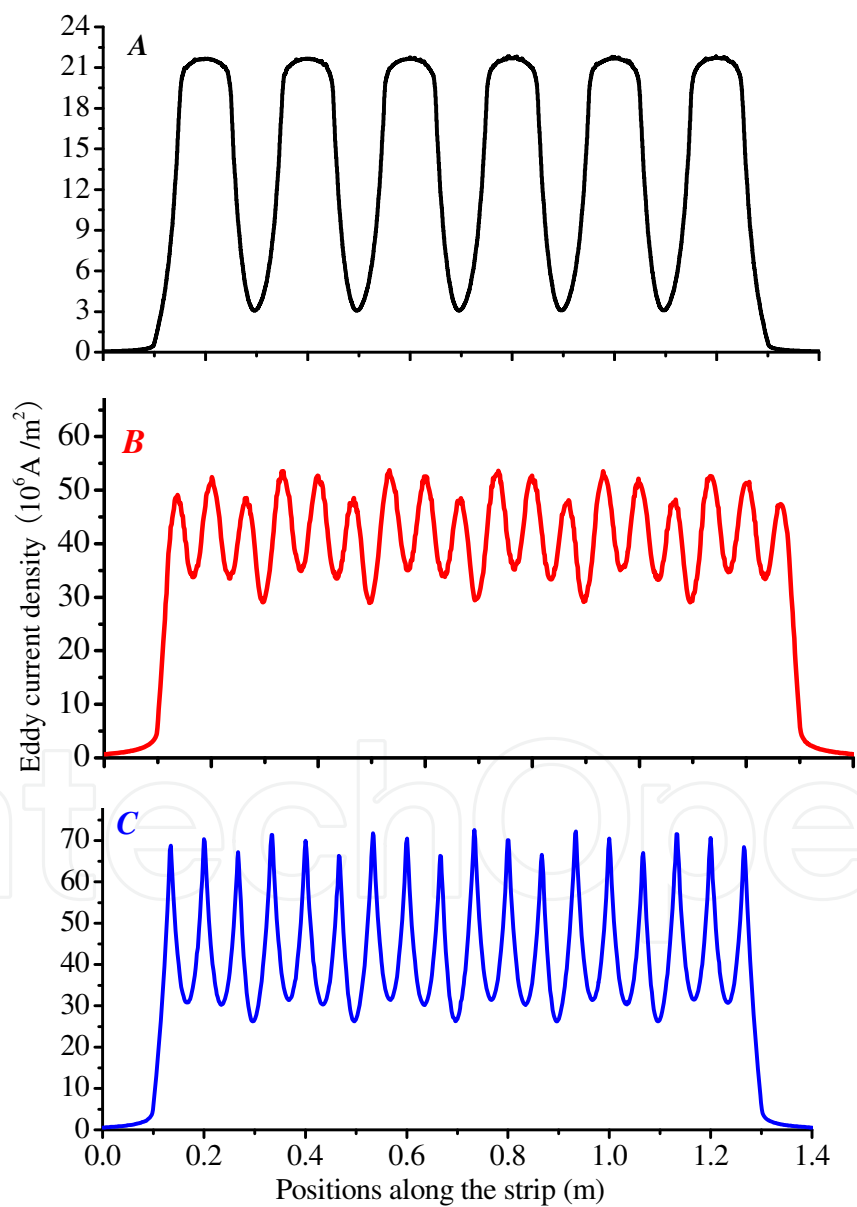

Fig. 20. The eddy current density distribution along the strip parallelly: (A) typical TWIH, (B) SW-TWIH and (C) improved SW-TWIH.
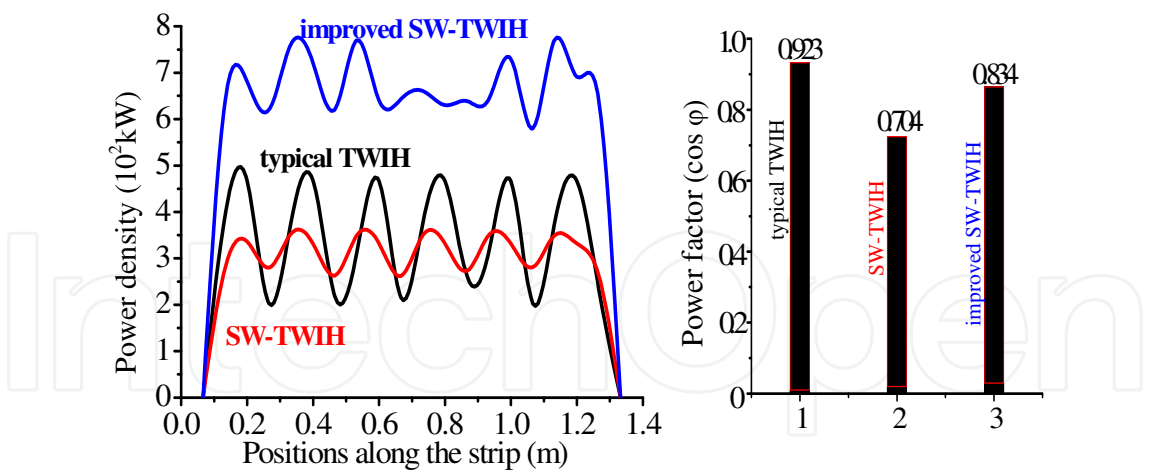
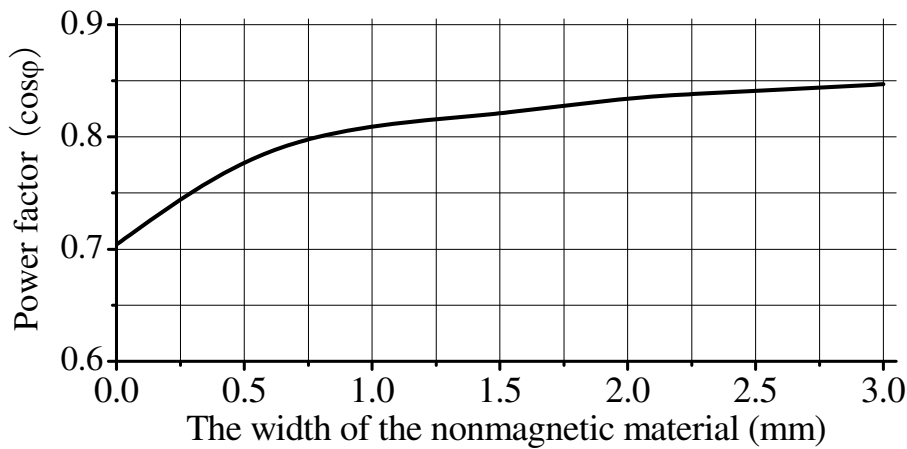Fig. 21. Relative power density distributions and the power factor.

Fig. 22. The power factor with different width of the nonmagnetic material.

4. Conclusion

The simulations have shown that a relative good power and eddy currents distribution across the strip can be obtained for both systems using the method of spatial control of the electromagnetic field. The theoretical values of efficiency (with uniform current density distribution in the inductor coil cross-section) are quite high for all the configurations. The TWIH systems, especially for the improved C-TWIH and the SW-TWIH systems, look to be more promising for further study because it might solve some problems related to metal deformation and noise from the system, which play important roles to the uniform of power and eddy currents. Moreover, the values of power density in the load are able to produce good heating of the strip.

Also, it is demonstrated that a convenient choice of the systems and their parameters (inductor geometry, poly-phase winding arrangement and supply, air gap values and control of the relative position of the inductors) gives the opportunity of obtaining very good energetic performances and a certain degree of control of the value and distribution of

the power transferred to the load. Some standard and specially developed FEM codes based on numerical methods were successfully used for the study of TWIH heaters. The main advantages and the particular characteristics of TWIH systems such as the effect of slots on induced power distributions were studied. The FEM codes and the results of numerical simulation may be therefore used easily and reliably, for the design of different TFIH systems.

It should be added that eddy current distributions and power intensity are not the only problems for the use of these systems and for this reason the comparison must be studied in depth. First of all, the electromagnetic problem solution must be coupled with the thermal and the mechanical ones in order to have a better understanding of the different temperature distributions, mechanical deformations and noise. Moreover an economic evaluation of the different power supply systems must be carried out.

5. Referring

We have referred many materials from the following papers we have published.

[1] Ho S. L., Wang Junhua, Fu W. N., Wang Y. H. "A novel crossed traveling wave induction heating system and finite element analysis of eddy current and temperature distributions," *IEEE Trans. Magn.,* vol: 45(10), pp: 4777-4780, Oct. 2009.

[2] J. H. Wang, S. L. Ho, W. N. Fu, Y. H. Wang "Design and analysis of a novel traveling wave induction heating system with magnetic slot wedges for heating moving thin strips ," *IEEE Trans. Magn.,* vol.20, no.6, pp. 2175 – 2178, 2010.

[3] Wang Junhua, Wang Youhua, "The study of two novel induction heating technology," *ICEMS 2008,* Oct. 17-20 2008, Wuhan China, pp: 572-574. .

[4] Wang Youhua, Wang Junhua, Li Jiangui, Li Haohua, "Analysis of induction heating eddy current distribution based on 3D FEM," *2008 IEEE Region 8 International Conference on Computational Technologies in Electrical and Electronics Engineering,* July 21-25 2008, Novosibirsk, RUSSIA, pp: 238-241.

[5] Yang Xiaoguang, Wang Youhua, "New Method for Coupled Field Analysis in Transverse Flux Induction Heating of Continuously Moving Sheet," *Heat Treatment of Metals,* vol.29, no.4, pp.53-57, 2004.

6. References

[1] A.L.Bowden, E.J.Davies, "Travelling Wave induction Heaters Design Considerations," *BNCE-UIE Electroheat for Metals Conference*, 11.5.2, Cambridge (England), 21-23 Sept. 1982

[2] S.Lupi, M.Forzan, F.Dughiero, et al. "In the corresponding TWIH system this problem is reduced since less and not sharp peaks are present with their highest," *IEEE Transactions on Magnetics*, 1999, vol35, no.5, pp.3556-3558.

[3] F.Dughiero, S.Lupi, P.Siega, "Analytical Calculation of Traveling Wave Induction Heating Systems," *International Symposium on Electromagnetic Fields in Electrical Engineering* 1993, 16-18 September 1993, Warsaw-Poland, 207-210.

[4] F.Dughiero, S.Lupi, V.Nemkov, et al. "Travelling wave inductors for the continuous induction heating of metal strips," *Proceedings of the Mediterranean Electrotechnical Conference-MELECON*.1994, vol.3 , no.3, pp.1154-1157.

[5] W. Andree, D. Schulze, Z. Wang , "3D FEM Eddy current computation in transverse flux induction heating equipment," *IEEE Transaction on Magnetic*, vol. 30, No.4, July 1994.

[6] Zanming Wang, Xiaoguang Yang, Youhua Wang, et al. "Eddy current and temperature field computation in transverse flux induction heating equipment," *IEEE Trans. Magn.*, vol. 37, no. 5, pp. 3437-3439, 2001.

[7] Z. Wang, X. Yang et al, " FEM Simulation of Transverse Flux Induction Heating for Galvanizing Line" Proceedings of the Fourth International Conference on Electromagnetic Field Problem and Applications.

[8] S. Lupi, M. Forzan, F. Dughiero, et al. "Comparison of edge-effects of transverse flux and travelling wave induction heating inductors," *IEEE Trans. Magn.*, vol. 35, no. 5, pp. 3556 -3558, 1999.

[9] F.Dughiero, S.Lupi, V.Nemkov, et al. "Travelling wave inductors for the continuous induction heating of metal strips," *Proceedings of the Mediterranean Electrotechnical Conference-MELECON*.1994, vol.3 , no.3, pp.1154-1157.

[10] A.Ali, V.Bukanin, F.Dughiero, et al. "Simulation of multiphase induction heating systems," *IEE Conference Publication*, 1994, vol.38, no.4, pp.211-214.

[11] V.V.Vadher, I.R.Smith. "Travelling Wave Induction Heaters with Compensating Windings", *ISEF"93, Warsaw (Poland)*. 16-18 Sept. 1993, pp. 211-217.

[12] X.G. Yang, Y.H. Wang, "The effect of coil geometry on the distributions of eddy current and temperature in transverse flux induction heating equipment," *Heat Treatment of Metals,* 2003, vol.28, no.7, pp.49-54.

[13] S. L. Ho, J. H. Wang, W. N. Fu, Y. H. Wang , "A novel crossed traveling wave induction heating system and finite element analysis of eddy current and temperature distributions," *IEEE Trans. Magn.*, vol. 45, no. 10, pp. 4777-4780, 2009.

[14] Nicola Bianchi, Fabrizio Dughiero, "Optimal design techniques applied to transverse-flux induction heating systems," *IEEE Trans. Magn.*, vol. 31, no. 3, pp. 1992-1995, 1995.

[15] Y. B. Li, S. L. Ho, W. N. Fu, W. Y. Liu, "An interpolative finite-element modeling and the starting process simulation of a large solid pole synchronous machine," *IEEE Trans. Magn.*, vol. 45, no. 10, pp. 4605-4608, 2009.
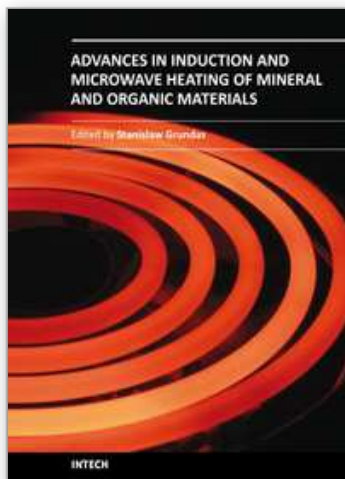
Advances in Induction and Microwave Heating of Mineral and Organic Materials

Edited by Prof. StanisÅ‚aw Grundas

ISBN 978-953-307-522-8

Hard cover, 752 pages

Publisher InTech

Published online 14, February, 2011

Published in print edition February, 2011

The book offers comprehensive coverage of the broad range of scientific knowledge in the fields of advances in induction and microwave heating of mineral and organic materials. Beginning with industry application in many areas of practical application to mineral materials and ending with raw materials of agriculture origin the authors, specialists in different scientific area, present their results in the two sections: Section 1-Induction and Microwave Heating of Mineral Materials, and Section 2-Microwave Heating of Organic Materials.

How to reference

In order to correctly reference this scholarly work, feel free to copy and paste the following:

Youhua Wang, Junhua Wang, S. L. Ho, Xiaoguang Yang, and W. N. Fu (2011). Two Novel Induction Heating Technologies: Transverse Flux Induction Heating and Travelling Wave Induction Heating, Advances in Induction and Microwave Heating of Mineral and Organic Materials, Prof. StanisÅ‚aw Grundas (Ed.), ISBN: 978-953-307-522-8, InTech, Available from: http://www.intechopen.com/books/advances-in-induction-and-microwave-heating-of-mineral-and-organic-materials/two-novel-induction-heating-technologies-transverse-flux-induction-heating-and-travelling-wave-induc

INTECH
open science | open minds